15.03.09 BI-TP 2009/07

The States of Matter in QCD

Helmut Satz

Fakultät für Physik, Universität Bielefeld, Germany

arXiv:0903.2778v1 [hep-ph] 16 Mar 2009

Abstract:

Quantum chromodynamics predicts that the interaction between its fundamental constituents, quarks and gluons, can lead to different states of strongly interacting matter, dependent on its temperature and baryon density. We first survey the possible states of matter in QCD and discuss the transition from a color-confining hadronic phase to a plasma of deconfined colored quarks and gluons. Next, we summarize the results from non-perturbative studies of QCD at finite temperature and baryon density, and address the origin of deconfinement in the different regimes. Finally, we consider possible probes to test the basic features of bulk matter in QCD.

1 States of Strongly Interacting Matter

What happens to strongly interacting matter in the limit of high temperatures and densities? This question has fascinated physicists ever since the discovery of the strong force and the multiple hadron production it leads to [1–5]. Let us look at some of the features that have emerged over the years.

- Hadrons have an intrinsic size, with a radius $r_h \simeq 1$ fm, and hence a hadron needs a space of volume $V_h \simeq (4\pi/3)r_h^3$ in order to exist. This suggests a limiting density $n_c = 1/V_h \simeq 2.4$ fm^{-3} of hadronic matter [3]. Beyond this point, hadrons overlap more and more, so that eventually they cannot be identified any more.
- Hadronic interactions provide abundant resonance production, and the resulting number $\rho(m)$ of hadron species increases exponentially as function of the resonance mass m, $\rho(m) \sim \exp(b\,m)$. Such a form for $\rho(m)$ appeared first in the statistical bootstrap model, based on self-similar resonance formation or decay [5]. It was then also obtained in the more dynamical dual resonance approach, which specifies the scattering matrix through its pole structure [6]. In hadron thermodynamics, the exponential increase of the resonance degeneracy is found to result in an upper limit for the temperature of hadronic matter, $T_c = 1/b \simeq 150 - 200$ MeV [5].
- What happens beyond T_c? In QCD, the hadrons are dimensionful color-neutral bound states of the more basic pointlike colored quarks and gluons. Hadronic matter, consisting of colorless constituents of hadronic dimensions, can therefore turn at high temperatures and/or densities into a quark-gluon plasma of pointlike colored quarks and gluons as constituents [7]. This deconfinement transition leads to a color-conducting state and thus is the QCD counterpart of the insulator-conductor transition in atomic matter [8].
- A further transition phenomenon, also expected from the behavior of atomic matter, is a shift in the effective constituent mass. At $T = 0$, in vacuum, quarks dress themselves with gluons to form the constituent quarks that make up hadrons. As a result, the bare quark mass $m_q \simeq 0$ is replaced by a constituent quark mass $M_q \sim 300$ MeV. In a hot medium, this dressing melts and $M_q \to m_q$. Since the QCD Lagrangian for $m_q = 0$ is chirally symmetric, $M_q \neq 0$ implies spontaneous chiral symmetry breaking. The melting $M_q \to 0$ thus corresponds to chiral symmetry restoration. We shall see later on that in QCD, as in atomic physics, the shift of the constituent mass coincides with the onset of conductivity.
- So far, we have considered the "heating" of systems of low or vanishing baryon number density. The compression of baryonic matter at low temperature could result in a third type of transition. This would set in if an attractive interaction between quarks in the deconfined baryon-rich phase results in the formation of colored bosonic diquark pairs, the counterpart of Cooper pairs in QCD. At sufficiently low temperature, these diquarks can then condense to form a color superconductor. Heating will dissociate the diquark pairs and turn the color superconductor into a normal color conductor.
- For a medium of quarks with color and flavor degrees of freedom, the diquark state can in fact consist of phases of different quantum number structures [9]. We also note that for increasing baryon density, the transition at low T could lead to an intermediate

"quarkyonic" state, in which baryons dissolve into quarks, but mesons remain as confined states [10,11]. In the present survey, we shall not pursue these interesting aspects any further.

Using the baryochemical potential μ as a measure for the baryon density of the system (i.e., for the total number of baryons minus that of antibaryons, per unit volume), we then expect the phase diagram of QCD to have the general schematic form shown in Fig. 1. Given QCD as the fundamental theory of strong interactions, we can use the QCD Lagrangian as dynamics input to derive the resulting thermodynamics of strongly interacting matter. For vanishing baryochemical potential, $\mu = 0$, this can be evaluated with the help of the lattice regularisation, leading to finite temperature lattice QCD.

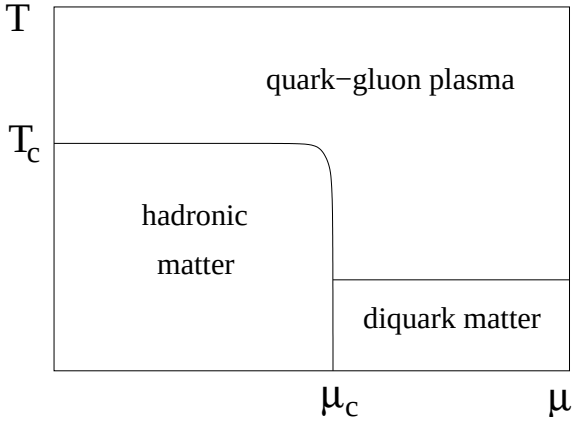

Figure 1: The phase diagram of QCD

2 From Hadrons to Quarks and Gluons

Before turning to the study of strongly interacting matter in QCD, we illustrate the transition from hadronic matter to quark-gluon plasma by a very simple model. For an ideal gas of massless pions, the pressure as function of the temperature is given by the Stefan-Boltzmann form

$$P_\pi = 3\frac{\pi^2}{90}T^4 \tag{1}$$

where the factor 3 accounts for the three charge states of the pion. The corresponding form for an ideal quark-gluon plasma with two flavors and three colors is

$$P_{qg} = \{2\times 8 + \frac{7}{8}(3\times 2\times 2\times 2)\}\frac{\pi^2}{90}T^4 - B = 37\,\frac{\pi^2}{90}T^4 - B. \tag{2}$$

In Eq. (2), the first term in the curly brackets accounts for the two spin and eight color degrees of freedom of the gluons, the second for the three color, two flavor, two spin and two particle-antiparticle degrees of freedom of the quarks, with 7/8 to obtain the correct statistics. The bag pressure B [12] takes into account the (non-perturbative) difference between the physical vacuum and the ground state for colored quarks and gluons [13].

Since in thermodynamics, a system chooses the state of lowest free energy and hence highest pressure, we compare in Fig. 2 a the temperature behavior of Eq's. (1) and (2). Our simple

model thus leads to a two-phase picture of strongly interacting matter, with a hadronic phase up to

$$T_c = \left(\frac{45}{17\pi^2}\right)^{1/4} B^{1/4} \simeq 0.72\ B^{1/4} \tag{3}$$

and a quark gluon plasma above this critical temperature. From hadron spectroscopy, the bag pressure is given by $B^{1/4} \simeq 0.2$ GeV, so that we obtain

$$T_c \simeq 150 \text{ MeV} \tag{4}$$

as the deconfinement temperature. In the next section we shall find this simple estimate to be remarkably close to the value obtained in lattice QCD.

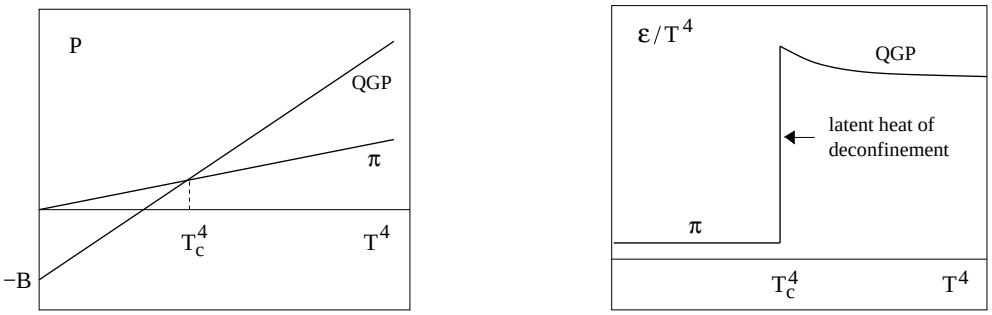

(a) (b)

Figure 2: Pressure and energy density in a two-phase ideal gas model.

The energy densities of the two phases of our model are given by

$$\epsilon_\pi = \frac{\pi^2}{10} T^4 \tag{5}$$

and

$$\epsilon_{qg} = 37\frac{\pi^2}{30} T^4 + B. \tag{6}$$

By construction, the transition is first order, and the resulting temperature dependence is shown in Fig. 2 b. At T_c, the energy density increases abruptly by the latent heat of deconfinement, $\Delta\epsilon$. Using eq. (3), its value is found to be

$$\Delta\epsilon = \epsilon_{qg}(T_c) - \epsilon_\pi(T_c) = 4\,B, \tag{7}$$

so that it is determined completely by the bag pressure measuring the level difference between physical and colored vacua.

For an ideal gas of massless constituents, the trace $\epsilon - 3P$ of the energy-momentum tensor quite generally vanishes. Nevertheless, in our model of the ideal plasma of massless quarks and gluons, we have for $T \geq T_c$

$$\epsilon - 3P = 4\,B, \tag{8}$$

again specified by the bag pressure and not zero. This is related to the so-called trace anomaly and indicates the dynamical generation of a dimensional scale; we shall return to it in the next section, where we will find that this scale is set by the vacuum expectation value of the gluon condensate.

3 Matter at Finite Temperature

We now want to show that the conceptual considerations of the last section indeed follow from strong interaction thermodynamics as based on QCD as the input dynamics. QCD is defined by the Lagrangian

$$\mathcal{L} \;=\; -\frac{1}{4}F^a_{\mu\nu}F^{\mu\nu}_a \;-\; \sum_f \bar{\psi}^f_\alpha (i\gamma^\mu\partial_\mu + m_f - g\gamma^\mu A_\mu)^{\alpha\beta}\psi^f_\beta \;, \tag{9}$$

with

$$F^a_{\mu\nu} \;=\; (\partial_\mu A^a_\nu - \partial_\nu A^a_\mu - g f^a_{bc} A^b_\mu A^c_\nu) \;. \tag{10}$$

Here A^a_μ denotes the gluon field of color a (a=1,2,...,8) and ψ^f_α the quark field of color α (α=1,2,3) and flavor f; the input ('bare') quark masses are given by m_f, and g is a dimensionless coupling. With the dynamics thus determined, the corresponding thermodynamics is obtained from the partition function, which is most suitably expressed as a functional path integral,

$$Z(T,V) = \int\; dA\; d\psi\; d\bar{\psi}\; \exp\;\left(-\int_V d^3x \int_0^{1/T} d\tau\; \mathcal{L}(A,\psi,\bar{\psi})\;\right), \tag{11}$$

since this form involves directly the Lagrangian density defining the theory. The spatial integration in the exponent of Eq. (11) is performed over the entire spatial volume V of the system; in the thermodynamic limit it becomes infinite. The time component x_0 is "rotated" to become purely imaginary, $\tau = ix_0$, thus turning the Minkowski manifold, on which the fields A and ψ are originally defined, into a Euclidean space. The integration over τ in Eq. (11) runs over a finite slice whose thickness is determined by the temperature of the system; the vector (spinor) fields have to be periodic (antiperiodic) at the boundary $\tau = 0, \beta$.

From $Z(T,V)$, all thermodynamical observables can be calculated in the usual fashion. Thus

$$\epsilon = \left(\frac{T^2}{V}\right)\left(\frac{\partial \ln Z}{\partial T}\right)_V \tag{12}$$

gives the energy density, and

$$P = T\left(\frac{\partial \ln Z}{\partial V}\right)_T \tag{13}$$

the pressure. For the study of critical behavior, long range correlations and multi-particle interactions are of crucial importance; hence perturbation theory cannot be used. The necessary non-perturbative regularisation scheme is provided by the lattice formulation of QCD [14]; it leads to a form which can be evaluated numerically by computer simulation [15].

The calculational methods and techniques of finite temperature lattice QCD form a challenging subject on its own, which certainly surpasses the scope of this survey. We therefore restrict ourselves here to a summary of the main conceptual results obtained so far; for more details, we refer to the corresponding chapter of this handbook as well as to other excellent books and reviews [16].

The first variable considered in finite temperature lattice QCD is the deconfinement measure provided by the Polyakov loop [17, 18]

$$L(T) \sim \lim_{r\to\infty}\; \exp\{-F(r)/T\} \tag{14}$$

where $F(r)$ is the free energy of a static quark-antiquark pair separated by a distance r. In pure gauge theory, without light quarks, $F(r) \sim \sigma r$, where σ is the string tension; hence here $F(\infty) = \infty$, so that $L = 0$. In a deconfined medium, color screening among the gluons leads to a melting of the string, which makes $F(r)$ finite at large r; hence now L does not vanish. It thus becomes an 'order parameter' like the magnetisation in the Ising model: for the temperature range $0 \leq T \leq T_L$, we have $L = 0$ and hence confinement, while for $T_L < T$ we have $L > 0$ and deconfinement; see Fig. 3. The temperature T_L at which L becomes finite thus defines the onset of deconfinement.

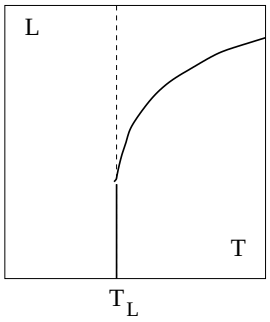

Figure 3: The temperature dependence of the Polyakov loop in pure $SU(3)$ gauge theory.

In the large quark mass limit, QCD reduces to pure $SU(3)$ gauge theory, which is invariant under a global Z_3 symmetry. The Polyakov loop provides a measure of the state of the system under this symmetry: it vanishes for Z_3 symmetric states and becomes finite when Z_3 is spontaneously broken. Hence the critical behavior of $SU(3)$ gauge theory is in the same universality class as that of Z_3 spin theory (the 3-state Potts model): both are due to the spontaneous symmetry breaking of a global Z_3 symmetry, leading to a first order phase transition [19].

For finite quark mass m_q, $F(r, T)$ remains finite for $r \to \infty$, since the 'string' between the two color charges 'breaks' when the corresponding potential energy becomes equal to the mass M_h of the lowest hadron; beyond this point, it becomes energetically more favourable to produce an additional hadron. Hence now L no longer vanishes in the confined phase, but only becomes exponentially small there,

$$L(T) \sim \exp\{-M_h/T\}; \tag{15}$$

here M_h is a typical hadron mass, of the order of 0.5 to 1.0 GeV, so that at $T_c \simeq 170$ MeV, $L \sim 10^{-2}$, rather than zero. Deconfinement is thus indeed much like the insulator-conductor transition, for which the order parameter, the conductivity $\sigma(T)$, also does not really vanish for $T > 0$, but with $\sigma(T) \sim \exp\{-\Delta E/T\}$ is only exponentially small, since thermal ionisation (with ionisation energy ΔE) produces a small number of unbound electrons even in the insulator phase.

Fig. 4 a illustrates the schematically the behavior of $L(T)$ and of the corresponding susceptibility $\chi_L(T) \sim \langle L^2 \rangle - \langle L \rangle^2$, as obtained in finite temperature lattice studies [20–22], for the case of two flavors of light quarks. We note that $L(T)$ undergoes the expected sudden increase from a small confinement to a much larger deconfinement value. The sharp peak

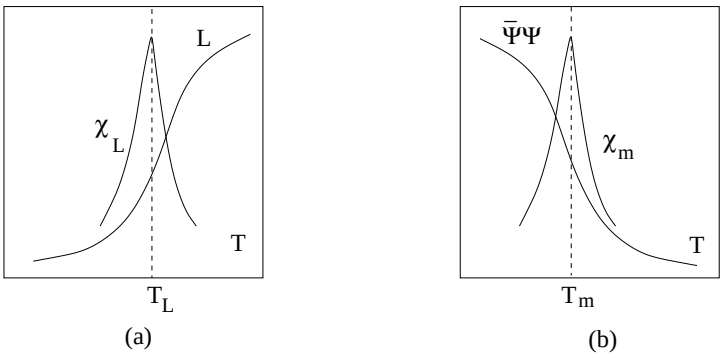

Figure 4: Schematic view of the temperature dependence of the Polyakov loop and of the chiral condensate, for $N_f = 2$ and small finite quark mass.

of $\chi_L(T)$ defines quite well a transition temperature T_L, which we shall shortly specify in physical units.

The next quantity to consider is the effective quark mass; it is measured by the expectation value of the corresponding term in the Lagrangian, $\langle\bar{\psi}\psi\rangle(T)$. In the limit of vanishing current quark mass, the Lagrangian becomes chirally symmetric and $\langle\bar{\psi}\psi\rangle(T)$ the corresponding order parameter. In the confined phase, with effective constituent quark masses $M_q \simeq 0.3$ GeV, this chiral symmetry is spontaneously broken, while in the deconfined phase, at high enough temperature, we expect its restoration. Hence now $\langle\bar{\psi}\psi\rangle(T)$ constitutes a genuine order parameter, finite for $T < T_m$ and vanishing for $T \geq T_m$, as shown in Fig. 5.

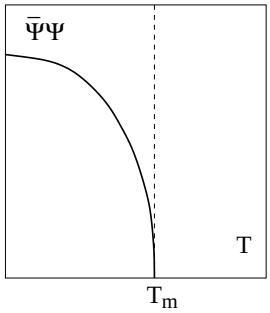

Figure 5: The temperature dependence of the chiral condensate in the limit $m_q = 0$.

In the real world, with finite pion and hence finite current quark mass, this symmetry is also only approximate, since $\langle\bar{\psi}\psi\rangle(T)$ now never vanishes at finite T. The behavior of $\langle\bar{\psi}\psi\rangle(T)$ and of the corresponding susceptibility $\chi_m \sim \partial\langle\bar{\psi}\psi\rangle/\partial m_q$ are illustrated in Fig. 4 b, again for two light quark flavors. We note here the expected sudden drop of the effective quark mass and the associated sharp peak in the susceptibility. The temperature T_m at which this occurs is generally found to coincide with the T_L obtained through the deconfinement measure, leading to the conclusion that that at vanishing baryon number density, quark deconfinement and the shift from constituent to current quark mass define the same transition temperature T_c. However, one lattice group [23] has recently found indications for two distinct transitions, with chiral symmetry being restored (at about 150 MeV) slightly before deconfinement occurs (at about 175 MeV). Such a behavior is very difficult to accommodate in most conventional confinement scenarios and hence must be investigated further.

We thus obtain for $\mu_B = 0$ a rather well defined phase structure, consisting of a confined phase for $T < T_c$, with $L(T) \simeq 0$ and $\langle\bar{\psi}\psi\rangle(T) \neq 0$, and a deconfined phase for $T > T_c$ with $L(T) \neq 0$ and $\langle\bar{\psi}\psi\rangle(T) \simeq 0$. The underlying symmetries associated to the critical behavior at $T = T_c$, the Z_3 symmetry of deconfinement and the chiral symmetry of the quark mass shift, become exact in the limits $m_q \to \infty$ and $m_q \to 0$, respectively. In the real world, both symmetries are only approximate; nevertheless, even for not too large finite quark masses, both associated measures retain an almost critical behavior.

Next we turn to the behavior of energy density ϵ at deconfinement [24]. In Fig. 6, it is seen that for two light and one heavy quark flavors, ϵ/T^4 changes quite abruptly at the above critical temperature T_c, increasing from a low hadronic value to one slightly below that expected for an ideal gas of massless quarks and gluons [22, 24, 25].

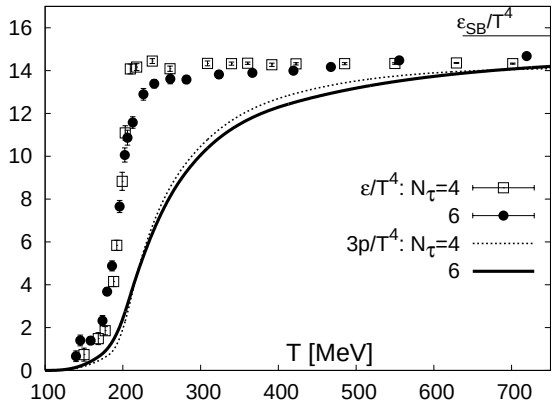

Figure 6: Energy density and pressure vs. temperature [22]

What is the value of the transition temperature? Since QCD (in the limit of massless quarks) does not contain any dimensional parameters, T_c can only be obtained in physical units by expressing it in terms of some other known observable which can also be calculated on the lattice, such as the ρ-mass or the proton mass; more recently, the mass splitting of quarkonium states [26] and the pion decay constant f_π [23] were used to gauge the lattice scale. Extrapolating the lattice results [26] to the continuum limit and using charmonium splitting as scale led to $T_c \simeq 170 - 190$ MeV, while the results of [23], with two transitions, gave with f_π as scale about 150 MeV for chiral symmetry restoration and 175 MeV for deconfinement.

Related to the sudden increase of the energy density at deconfinement, there are two further points to note. In the region $T_c < T < 2\ T_c$, there still remain strong interaction effects: the pressure does not show the same temperature dependence as ϵ, and hence the 'interaction measure' $\Delta = (\epsilon - 3P)/T^4$, shown in Fig. 7, is sizeable and does not vanish, as it would for an ideal gas of massless constituents. In the simple model of the previous section, this effect arose due to the bag pressure, measuring the difference between the physical and the "colored" vacuum, and in actual QCD, one can also interpret it in such a fashion [13]. More generally, it follows from the so-called trace anomaly of QCD; let us consider this in a little more detail.

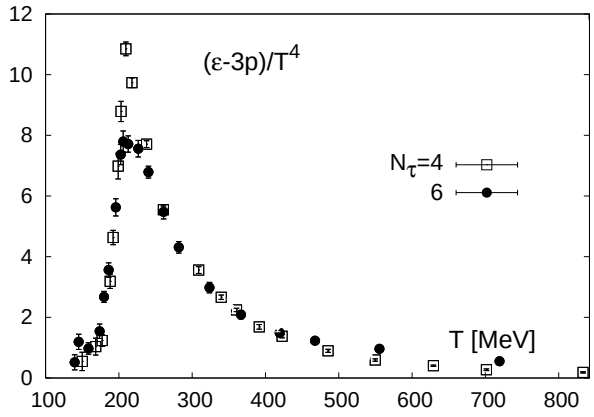

Figure 7: Interaction measure vs. temperature for two light and one heavy quark flavors [22]

As already noted, the QCD Lagrangian is scale-invariant: in the case of massless quarks and gluons it contains no dimensional scale. Any dimensional observable must therefore be measurable in terms of the temperature, and so the trace of the energy-momentum tensor must be proportional to T^4: $\epsilon - 3P \sim T^4$. This in turn implies that for $T \to 0$, it should vanish. However, the vacuum expectation value of the gluon sector,

$$G_0^2 \equiv \langle 0|F_{\mu\nu}^a F_a^{\mu\nu}|0\rangle, \tag{16}$$

does not vanish there. Instead, it measures the sea of virtual gluons, the gluon condensate, which defines the difference between the colored system and the physical vacuum. This anomalous behavior was accounted above through the bag pressure, and the numerical value of G_0^2 or B can only be determined ("gauged") empirically, the theory itself being scale-invariant. In the MIT bag model [12], one obtains

$$R_N = \left(\frac{3}{2\pi B}\right)^{1/4} = \left(\frac{6}{\pi G_0^2}\right)^{1/4} \tag{17}$$

for the radius of a nucleon. For $R_N = 1$ fm, this leads to $4B = G_0^2 \simeq 1$ GeV/fm^3. There are various more refined estimates for the gluon condensate at $T = 0$, determined by different non-perturbative hadronic inputs [27], giving a rather wide range of values, $G_0^2 \simeq 1 - 2$ GeV/fm^3 [28,29]. In any case, to recover the correct vacuum physics, the trace of the energy momentum tensor must be renormalized [29], giving

$$\epsilon - 3P = G_0^2 - G_T^2, \tag{18}$$

where G_T^2 is the expectation value of the gluon condensate at temperature T. In the confinement region $T \leq T_c$, the latter is found to remain close to G_0^2 [30,31], leading to $\epsilon - 3P \simeq 0$, until the temperature approaches the deconfinement point. There G_T^2 drops suddenly, i.e., the gluon condensate "melts" and as a consequence, the interaction measure shows a rapid rise, as seen in Fig. 7. We thus find once again that the temperature change of the gluon condensate determines the specific heat of deconfinement: it appears that deconfinement corresponds to the melting of the gluon condensate.

The second point to note is that the thermodynamic observables remain about 10 % below their Stefan-Boltzmann values (marked "SB" in Fig. 6) even at very high temperatures, where the interaction measure becomes very small. Such deviations from ideal gas behavior can be modelled in terms of effective 'thermal' masses $m_{\rm th}$ of quarks and gluons, with $m_{\rm th} \simeq g(T)\,T$ [32, 33]. Maintaining the next-to-leading order term in mass in the Stefan-Boltzmann form gives for the pressure

$$P = c\,T^4 \left[1 - a\left(\frac{m_{\rm th}}{T}\right)^2\right] = c\;T^4[1 - a\;g^2(T)] \tag{19}$$

and for the energy density,

$$\epsilon = 3\,c\,T^4 \left[1 - \frac{a}{3}\left(\frac{m_{\rm th}}{T}\right)^2 - \frac{2a\,m_{\rm th}}{3\,T}\left(\frac{\partial m_{\rm th}}{\partial T}\right)\right] = 3\,c\,T^4 \left[1 - a\,g^2(T) - \frac{2a\,m_{\rm th}}{3}\left(\frac{\partial g}{\partial T}\right)\right], \tag{20}$$

where c and a are color- and flavor-dependent positive constants. Since $g^2(T) \sim 1/\ln T$, we then obtain

$$\Delta = -2c\,a\,m_{\rm th}\left(\frac{\partial g}{\partial T}\right) = -c\,a\,\left(\frac{\partial g^2}{\partial \ln T}\right) \sim -g^4 \tag{21}$$

for the interaction measure. The deviations of P/T^4 and ϵ/T^4 from the massless Stefan-Boltzmann form thus vanish as $g^2 \sim (\log\ T)^{-1}$, while the interaction measure decreases more rapidly, vanishing as $g^4 \sim (\log\ T)^{-2}$. From eq. (21) we also see that it is the running in T of the coupling which brings in and describes the interaction; for a coupling "constant", we would have $\Delta = 0$.

In summary, finite temperature lattice QCD at vanishing overall baryon density shows

- that there is a transition leading to color deconfinement, coincident with chiral symmetry restoration, at the temperature $T_c \simeq 0.15$ - 0.20 GeV;
- that this transition is accompanied by a sudden increase in the energy density (the "latent heat of deconfinement") from a small hadronic value to a much larger value, about 10 % below that of an ideal quark-gluon plasma.

In the two following sections, we want to address in more detail the nature of the critical behavior encountered at the transition.

4 The Order of the Transition

We address here first the behavior of systems of vanishing overall baryon density ($\mu = 0$) and come to the situation for $\mu \neq 0$ at the end. Consider the case of three quark species $u,\ d,\ s$.

- In the limit $m_q \to \infty$ for all quark species, we recover pure $SU(3)$ gauge theory, with a deconfinement phase transition provided by spontaneous Z_3 breaking. It is first order, as is the case for the corresponding spin system, the 3-state Potts model [19].
- For $m_q \to 0$ for all quark masses, the Lagrangian becomes chirally symmetric, so that we have a phase transition corresponding to chiral symmetry restoration. In the case of three massless quarks, the transition is also of first order [34].

- For $m_{u,d} = 0$ and $m_s > m_s^{\rm tri}$, the transition is of second order and presumably in the $O(4)$ universality class [34]. The second order limits of the first order regions appear to be in the Ising (Z_2) universality class [35]. At the tricritical point $m_s^{\rm tri}$, the two different continuous transitions meet with the first order transition [36].

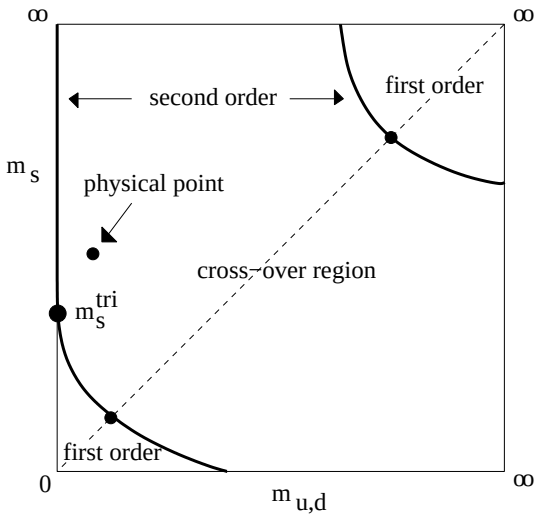

Figure 8: The form of thermal critical behavior in QCD

- For $0 < m_q < \infty$, there is neither spontaneous Z_3 breaking nor chiral symmetry restoration. Hence in general, there is no singular behavior, apart from the transient disappearence of the first order discontinuities on a line of second order transitions. Beyond this, there is no genuine phase transition, but only a "rapid cross-over" from confinement to deconfinement. The overall behavior is summarized in Fig. 8.
- As already implicitely noted above, both "order parameters" $L(T)$ and $\chi(T)$ nevertheless show a sharp temperature variation for all values of m_q, so that it is in fact possible to define quite well a common cross-over point T_c.
- The nature of the transition thus depends quite sensitively on the number of flavors N_f and the quark mass values: it can be a genuine phase transition (first order or continuous), or just a rapid cross-over. The case realized in nature, the "physical point", corresponds to small u, d masses and a larger s-quark mass. It is fairly certain today that this point falls into the cross-over region.

Before turning to the behavior at finite baryon density, we want to consider a particular consequence of the transition order. The standard way to determine the order is a study of the temperature dependence of the relevant order parameter; alternatively, one may check the behavior of the energy density in the critical region. Another, particularly instructive test is the speed of sound in the interacting medium. It is defined as

$$c_s^2(T) = \left(\frac{\partial P}{\partial \epsilon}\right)_V = \left(\frac{\partial P}{\partial T}\right)_V \Big/ \left(\frac{\partial \epsilon}{\partial T}\right)_V \tag{22}$$

and measures the relative change of the pressure compared to that of the energy density. For an ideal gas of massless constituents, $c_s^2 = 1/3$. In the confined state, we expect the system

to behave like an ideal resonance gas, which for an exponentially increasing resonance mass spectrum $\rho(m) \sim \exp\{b\, m\}$ leads to critical behavior at $T = T_c = 1/b$. Very near T_c, any further energy input goes into the production of more and heavier resonances, not into kinetic energy, and hence c_s^2 has a pronounced minimum or vanishes at T_c. In lattice studies [37], there are indications of such behavior, with c_s^2 dropping as $T \to T_c$ both from below and from above T_c. In the deconfined state, the decrease is physically less well understood. The pattern is illustrated in Fig. 9.

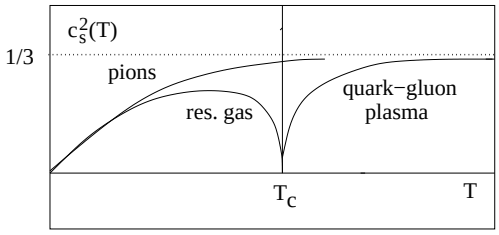

Figure 9: The speed of sound in QGP matter, compared to the behavior of an ideal pion gas

Finally we want to consider the general phase diagram, allowing a non-vanishing baryon density ($\mu \neq 0$), assuming the number of baryons exceeds that of antibaryons. Here diverse general arguments [38] suggest for two light and one heavy quark flavors a phase diagram of the form shown in Fig. 10. It shows non-singular behavior in a region between $0 \leq \mu < \mu_c$, a critical point at μ_c, and beyond this a first order transition. Unfortunately, for $\mu \neq 0$ the conventional computer algorithms of lattice QCD break down, and hence new calculation methods have to be developed. First such attempts (reweighting [39] or power series [40,41]) are in accord with expected pattern; thus the convergence radius of the power series expansion does seem to be bounded. Further recent lattice calculation provide additional support; as shown in Fig. 11, the baryon density fluctuations appear to diverge for some critical value of the baryochemical potential [40, 41]. On the other hand, analytic continuation methods [42, 43] leave open the existence of any critical behavior at finite μ.

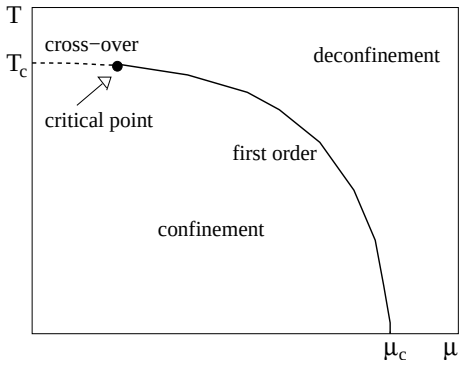

Figure 10: Phase structure in terms of the baryon density

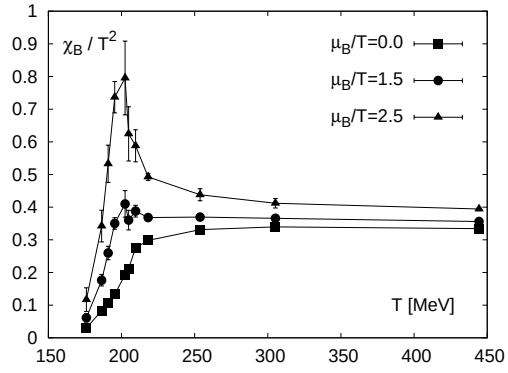

Figure 11: Baryon number susceptibility χ_q vs. temperature [40]

We conclude then that the critical behavior for strongly interacting matter at low or vanishing baryon density, describing the onset of confinement in the early universe as well as in high

energy nuclear collisions, occurs in the rather enigmatic form of a "rapid cross-over". There is no thermal singularity and hence, in a strict sense, there are neither distinct states of matter nor phase transitions between them. So what does the often mentioned experimental search for a "new state of matter" really mean? How can a new state appear without a phase transition? Is there a more general way to define and distinguish different states of bulk media? After all, in statistical QCD one does find that thermodynamic observables – energy and entropy densities, pressure, as well as the "order parameters" $L(T)$ and $\chi(T)$ – continue to change rapidly and thus define a rather clear transition line in the entire cross-over region. Why is this so, what is the mechanism which can cause such a transition?

5 The Origin of the Transition

In the present section, we want consider a speculative answer to this rather fundamental question [44], starting again with the case of vanishing baryon density. The traditional phase transitions, such as the freezing of water or the magnetization of iron, are due to symmetry breaking and the resulting singularities of the partition function. But there are other "transitions", such as making pudding or boiling an egg, where one also has two clearly different states, but no singularities in the partition function. Such "liquid-gel" transitions are generally treated in terms of cluster formation and percolation [45]. They also correspond to critical behavior, but the quantities that diverge are geometric (cluster size) and cannot be obtained from the partition function.

The simplest example of this phenomenon is provided by two-dimensional disk percolation. One distributes small disks of area $a = \pi r^2$ randomly on a large surface $A = \pi R^2$, $R \gg r$, with overlap allowed. With an increasing number of disks, clusters begin to form. Given N disks, the disk density is $n = N/A$. Clearly, the average cluster $S(n)$ size will increase with n. The striking feature is that it does so in a very sudden way (see Fig. 12); as n approaches some "critical value" n_c, $S(n)$ suddenly becomes large enough to span the surface A. In fact, in the limit $N \to \infty$ and $A \to \infty$ at constant n, both $S(n)$ and $dS(n)/dn$ diverge for $n \to n_c$: we have percolation as a geometric form of critical behavior.

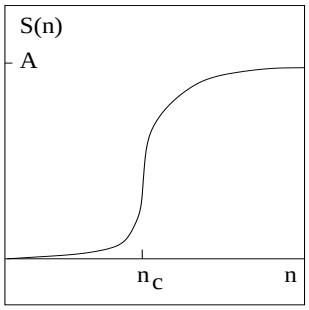

Figure 12: Cluster size $S(n)$ vs. density n

The critical density for the onset of percolation has been determined (numerically) for a variety of different systems. In two dimensions, disks percolate at $n_p \simeq 1.13/(\pi r^2)$, i.e., when we have a little more than one disk per unit area. Because of overlap, at this point only 68% of space is covered by disks, 32% remain empty. We therefore emphasize that n_p is only the

average overall density for the onset of percolation. The density in the largest and hence percolating cluster at this point must evidently be larger than $n_p/0.68 \simeq 1.66/\pi r^2$; it is in fact found to be $n_p^{\rm cl} \simeq 1.72/\pi r^2$ [46].

In three dimensions, the corresponding problem is one of overlapping spheres in a large volume. Here the critical density for the percolating spheres becomes $n_p \simeq 0.34/[(4\pi/3)r^3]$, with r denoting the radius of the little spheres now taking the place of the small disks we had in two dimensions. At the critical point in three dimensions, however, only 29% of space is covered by overlapping spheres, while 71% remains empty, and here both spheres and empty space form infinite connected networks. The density $n_p^{\rm cl}$ of the largest connected cluster at this point in overall density is thus much larger than $0.34/V_0$; in fact, it must exceed $1.17/V_0$.

Let us then consider hadrons of intrinsic size $V_h = (4\pi/3)r_h^3$, with $r_h \simeq 0.8$ fm. In three-dimensional space, the formation of a connected large-scale cluster first occurs at the overall average density

$$n_c = \frac{0.34}{V_h} \simeq 0.16 \text{ fm}^{-3}. \tag{23}$$

This point specifies the onset of large-scale connected strongly interacting matter, in contrast to a gas of hadrons. However, as we saw, the density of the largest matter clusters is much higher than the average value given by eq. (23), and assuming all non-empty space to form one cluster, we obtain $n_{\rm cl} \simeq 1.2/V_h \simeq 0.55$ fm^{-3} as (lower bound for the) critical density. Based on results for the two-dimensional case, we expect the threshold density $n_{\rm cl}$ to be about $(1.5 \text{ - } 2.0)/V_h \simeq (0.7-0.9)$ fm^{-3}. If we assume that at this point, the cluster is of an ideal gas of all known hadrons and hadronic resonances, then we can calculate the temperature of the gas at the density $n_{\rm cl}$: $n_{\rm res}(T = T_c) = n_{\rm cl}$ implies $T_c \simeq 170-190$ MeV, which agrees quite well with the value of the deconfinement temperature found in lattice QCD for $\mu = 0$. Cluster formation and percolation theory thus provide a possible tool to specify the deconfinement transition in strongly interacting matter.

Such considerations may in fact well be of a more general nature than the problem of states and transitions in strong interaction physics. The question of whether symmetry or connectivity (cluster formation) determines the different states of many-body systems has intrigued theorists in statistical physics for a long time [47]. The lesson learned from spin systems appears to be that cluster formation and the associated critical behavior are the more general features, which under certain conditions can also lead to thermal criticality, i.e., singular behavior of the partition function.

Next we turn to the more general phase structure as function of T and μ, as illustrated in Fig. 10. What conceptual aspects of hadronic interactions could lead to such behavior, and in particular, what features in hadronic dynamics result in the observed changes of the transition structure as function of baryon density?

At low baryon density, the constituents of hadronic matter are mostly mesons, and the dominant interaction is resonance formation; with increasing temperature, different resonance species of increasing mass are formed, leading to a gas of ever increasing degrees of freedom. They are all of a typical hadronic size (with a radius $R_h \simeq 1$ fm) and can overlap or interpenetrate each other. For $\mu \simeq 0$, the contribution of baryons/antibaryons and baryonic resonances is relatively small, but with increasing baryon density, they form an ever larger section of the

species present in the matter, and beyond some baryon density, they become the dominant constituents. Finally, at vanishing temperature, the medium consists essentially of nucleons.

At high baryon density, the dominant interaction is non-resonant. Nuclear forces are short-range and strongly attractive at distances of about 1 fm; but for distances around 0.5 fm, they become strongly repulsive. The former is what makes nuclei, the latter (together with Coulomb and Fermi repulsion) prevents them from collapsing. The repulsion between a proton and a neutron shows the purely baryonic "hard-core" effect and is connected neither to Coulomb repulsion nor to Pauli blocking of nucleons. As a consequence, the volumes of nuclei grow linearly with the sum of its protons and neutrons. With increasing baryon density, the mobility of baryons in the medium becomes strongly restricted by the presence of other baryons (see Fig. 13), leading to a "jammed" state in which each baryon can only move a small distance before being blocked by others [48].

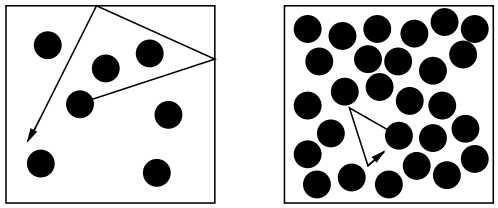

Figure 13: Hard sphere states: full mobility (a), "jammed" (b) [48]

To addresss the situation of high baryon density, we again turn to percolation theory, but now the constituents are hadrons containing a repulsive hard core, which we take for simplicity to be half that of the hadron. The percolation problem has been solved numerically for such a case as well [49]. We thus have two percolation scenarios [11]: one for the "bag fusion" of fully overlapping (or interpenetrating) mesonic spheres of radius $r_h \simeq 1$ fm, and one for baryons of the same radius, but having a hard core of radius $r_{hc} \simeq 0.5$ fm. In the $T - \mu$ plane, each percolation condition results in a transition curve, as illustrated in Fig. 14. As consequence, we have for low μ a mesonic bag fusion transition to a quark-gluon plasma, while for large μ, the baryonic percolation transition is the first to occur. It is thus quite conceivable that the competition between mesonic resonance clustering and the hard-core repulsion of baryons is at the origin of the different transition patterns in the $T-\mu$ plane. Extending such a scenario even further, one may also consider the large μ region of the $T - \mu$ plane below the mesonic transition curve to become a further "quarkyonic" state of matter [10].

6 Probing the States of Matter in QCD

We thus find that at sufficiently high temperatures and/or densities, strongly interacting matter will be in a new state, consisting of deconfined quarks and gluons. Is there some way of studying this state experimentally? The big bang theory for the creation and evolution of our universe implies that in its early stages, it must have consisted of deconfined quark and gluons. Neutron stars consist of very dense nuclear matter, and it is conceivable that they have quark matter cores. Both these possible applications are interesting, yet they do

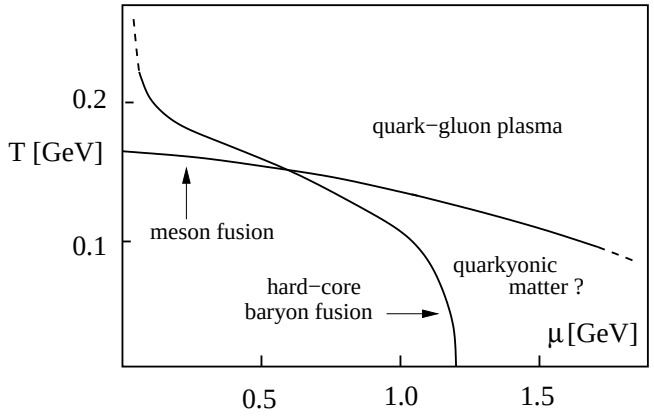

Figure 14: Fusion of mesonic bags vs. fusion of hard-core baryons [11]

not really allow a systematic study. The rapid growth which the field has experienced in the past two decades was to a very large extent stimulated by the idea that high energy nuclear collisions will produce droplets of strongly interacting matter - droplets large enough and long-lived enough to allow a study of the predictions which QCD makes for macroscopic systems. Moreover, it is expected that the conditions provided in these interactions will suffice for quark plasma formation. Hence the study of strongly interacting matter has today a multi-faceted experimental side; this, in turn, has stimulated much of the subsequent theoretical development.

The relevant experiments were initially denoted as ultra-relativistic nucleus-nucleus collisions; they are often, not quite correctly, also called heavy ion collisions (an ion fully stripped of its electrons is a nucleus). The studies began at Brookhaven National Laboratory (BNL) near New York and at the European Center for Nuclear Research (CERN) near Geneva around 1986/87. The first collisions had light nuclei (oxygen, silicon, sulphur) hitting heavy targets (gold, uranium), since light ions could be dealt with using injectors already existing at BNL and CERN. The successful analysis of these experiments provided the basis and motivation for the construction of new injectors of truly heavy nuclei, gold at BNL and lead at CERN; they came into operation in the middle 1990's. These early fixed target experiments were carried out at a center of mass energy of around 5 GeV per nucleon-nucleon collision at the BNL-AGS and around 20 GeV at the CERN-SPS. At the turn of millenium, the first dedicated nuclear accelerator, the Relativistic Heavy Ion Collider RHIC, started taking data at BNL, with a center of mass energy a factor ten higher, at 200 GeV per nucleon-nucleon collision. And coming soon now, the Large Hadron Collider LHC at CERN will bring the center-of-mass energy for nuclear collisions up to 5500 GeV, or 5.5 TeV.

The work of the different experimental groups working at these facilities has provided an immense wealth of data, and there is little doubt today that in such collisions comparatively large systems of higher energy density are formed than have ever been studied in the laboratory before. The detailed analyses of the results have also shown, however, that a number of new features arise, features which go beyond standard thermodynamics. Questions of non-equilibrium aspects, of thermalization, evolution and expansion, cooling, flow and many more make a direct application of equilibrium strong interaction thermodynamics anything but straight-forward. Nevertheless, it seems difficult to imagine that the more complex non-

equilibrium situation can be understood without having an understanding of the simpler equilibrium case. Our aim here is therefore to address some of the more general problems which arise when one tries to study a bubble of strongly interacting matter which is locally in equilibrium: what features allow us to determine the state of the matter inside such a bubble? We shall not address here the really fundamental question of how a nuclear collision can lead to equilibrated matter - this will be dealt with in other chapters of this handbook.

There are a number of methods we can use to analyse a sample of unknown strongly interacting matter:

- hadron radiation,
- electromagnetic radiation,
- dissociation of a passing quarkonium beam,
- energy loss of a passing hard jet.

The first two are *internal* probes, emitted by the thermal medium itself, while the latter are in a sense *external*: they are expected to be formed by very early hard interactions, before any thermal medium is established, and then test its features by how their behavior is modified through its presence. All methods will be dealt with in detail in this handbook. Here we just want to summarize the essential ideas.

6.1 Hadron Radiation

Consider a bubble of hot matter in a vacuum environment. Since the temperature of the bubble is by assumption much higher than that of the environment, it will radiate. Hadron radiation means that we study the emission of hadrons consisting of light (u, d, s) quarks; their size is given by the typical hadronic scale of about 1 fm $\simeq 1/(200$ MeV). Since they cannot exist inside a deconfined medium, they are formed at the transition surface between the hot matter and the physical vacuum. The physics of this surface is independent of the interior - the transition from deconfinement to confinement occurs at a temperature $T \simeq\ 160 - 190$ MeV, no matter how hot the medium initially was or still is in the interior of our volume. This is similar to having hot water vapor inside a glass container kept in a cool outside environment: at the surface, the vapor will condense into liquid, at a temperature of 100°C - independent of the temperature in the interior. As a result, studying soft hadron production in high energy collisions can provide us with information about the hadronization transition, but not about a hot QGP.

It should be noted here that the picture of a specific volume of hot matter, located in a vacuum and bounded by some surface, is just a cartoon to illustrate the relevant phenomena. From the point of view of statistical physics, one should rather consider an infinite hot medium adiabatically cooling off. Hadronization will then occur locally everywhere, once the evolution of the medium reaches the critical point in temperature.

The state of the medium formed at hadronization is evidently an interacting system of hadrons. If we consider the medium to be of low or even vanishing overall baryon density, the dominant interaction is resonance formation and decay. In this case, the interacting medium of basic hadrons (mainly pions, kaons, nucleons and anti-nucleons) can be replaced by an

ideal gas of all possible resonances, both mesonic and baryonic [50]. It was this concept that provided the basis for the statistical bootstrap approach [5] as well as of the dual-resonance model [6].

Assuming then that the hadronization process is the formation of an ideal hadronic resonance gas, the relative abundances of the different species are determined [51]. The partition function of such a gas is for $\mu = 0$ given by

$$\ln\ Z(T,V) = \sum_{\text{hadrons h}} \ln\ Z_h(T,V), \tag{24}$$

where

$$\ln\ Z_h(T,V) = d_h\ \frac{VT}{2\pi^2}\ m_h^2 K_2(m_h/T), \tag{25}$$

specifies the contribution of hadron or resonance species h, of mass m_h and (charge and spin) degeneracy d_h; we have here assumed Boltzmann statistics. In an ideal resonance gas of this type, the relative abundances of two species a and b are predicted to be

$$\frac{N_a}{N_b} = \frac{d_a m_a^2 K_2(m_a/T)}{d_b m_b^2 K_2(m_b/T)}; \tag{26}$$

conservation laws have to be taken into account where applicable. By studying the abundances of hadron species radiated by strongly interacting matter, we thus obtain information about the hadronization temperature.

One of the most striking observations in multihadron production in strong interaction physics is that the relative hadron abundances in all high energy collisions are correctly described by this approach, from e^+e^- annihilation to hadron-hadron and heavy ion interactions, and that they correspond to those of an ideal resonance gas at $T \simeq 170$ MeV [5,51]. On the other hand, this raises the question of how "thermal" hadronization actually occurs: in e^+e^- annihilation one cannot really consider the formation of strongly interacting "matter" as origin. Recent studies have therefore related thermal hadron production more generally to the existence of a color event horizon, allowing only tunnelling of thermal signals to the outside world [52]. This would make such production the QCD counterpart of Hawking-Unruh radiation from black holes [53].

Hadron radiation, as we have pictured it here, is oversimplified from the point of view of heavy ion interactions. In the case of static thermal radiation, at the point of hadronization all information about the earlier stages of the medium is lost, as we had noted above. If, however, the early medium has a very high energy density and can expand freely, i.e., is not constrained by the walls of a container, then this expansion will lead to a global hydrodynamic flow [54], giving an additional overall boost in momentum to the produced hadrons: they will experience a "radial flow" depending on the initial energy density. Moreover, if the initial conditions were not spherically symmetric, as is in fact the cases in peripheral heavy ion collisions, the difference in pressure in different spatial directions will lead to a further "directed" or "elliptic" flow. Both forms of flow thus do depend on the initial conditions. While the abundances of the species are not affected by such flow aspects, the different momentum distributions are and hence studies of hadron spectra can, at least in principle, provide information about the earlier, pre-hadronic stages.

6.2 Electromagnetic Radiation

The hot medium also radiates electromagnetically, i.e., it emits photons and dileptons (e^+e^- or $\mu^+\mu^-$ pairs) [55]. These are formed either by the interaction of quarks and/or gluons, or by quark-antiquark annihilation. Since the photons and leptons interact only electromagnetically, they will, once they are formed, leave the medium without any further modification. Hence their spectra provide information about the state of the medium at the place or the time they were formed, and this can be in its deep interior or at very early stages of its evolution. Photons and dileptons thus provide a possible probe of the hot QGP. The only problem is that they can be formed anywhere and at any time, also at later evolution stages and as well as through interaction or decay of the emitted hadrons. The task in making electromagnetic radiation a viable tool is therefore the identification of the hot "thermal" radiation indeed emitted by the QGP.

For the production of dilepton pair (for illustration, we consider $\mu^+\mu^-$) by a thermal medium, the lowest order process is quark-antiquark annihilation, as illustrated in Fig. 15. To calculate the mass spectrum of the emitted dileptons, the perturbative annihilation cross-section $\sigma(q\bar{q} \to \mu^+\mu^-)$ has to be convoluted by thermal quark and antiquark momentum distributions

$$f(k_q/T) \sim \exp\{-|k_q|/T\}, \tag{27}$$

where k_q is the three-momentum of the (massless) quark and T the temperature of the medium. We thus obtain

$$\frac{dN}{dM} \sim \int d^3k_q f(k_q) d^3k_{\bar{q}} f(k_{\bar{q}})\, \sigma(q\bar{q} \to \mu^+\mu^-), \tag{28}$$

where M is the invariant mass of the dilepton. The convolution leads to the schematic result

$$\frac{dN}{dM} \sim \exp\{-M/T\}, \tag{29}$$

so that a measurement of a thermal dilepton spectrum provides the temperature of the medium. As already indicated, if the medium undergoes an evolution (cooling), the observed dileptons originate from all stages, so that a temperature measurement is not straight-forward and will in general depend on the evolution pattern. In actual nuclear collision experiments, there is in addition competition from non-thermal dileptons (from hard primary Drell-Yan production at large M and from hadronic decays at lower M).

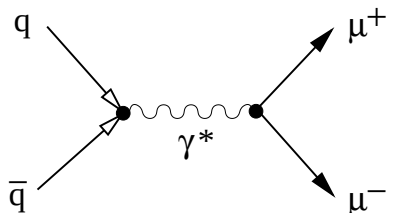

Figure 15: Dilepton production through $q\bar{q}$ annihilation

For photon production, the situation is similar. Here the dominant process is a gluonic Compton effect, as illustrated in Fig. 16. The rate is now given by a convolution of a

thermal quark with thermal gluon distribution, integrating over the perturbative Compton cross section $\sigma(qg \to q\gamma)$. The result is

$$\frac{dN}{d\omega} \sim \exp\{-\omega/T\}, \tag{30}$$

where $\omega = \sqrt{p_g^2}$ denotes the energy and p the momentum of the emitted gluon. Here again the two basic problems of electromagnetic probes arise: the thermal photons originate from all evolution stages and are in competition from non-thermal sources, both "prompt" hard photons and hadronic decay products.

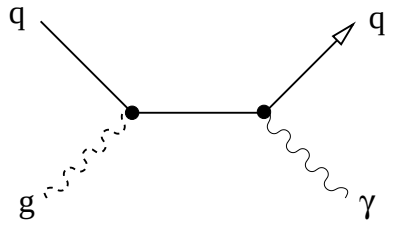

Figure 16: Photon production through gluonic Compton scattering

In either case the crucial signal to search for is a temperature-dependence of the mass or momentum spectra. If an increase of the parametric temperature of the spectra with collision energy could be found, these could indicate the production of media of increasing initial temperature.

6.3 Quarkonium Dissocation

The quark-gluon plasma consists by definition of deconfined and hence colored gluons, quarks and anti-quarks. One of the essential features of an electromagnetic plasma is Debye charge-screening, which reduces the long-range Coulomb potential in vacuum to a much shorter range screened in-medium form,

$$\frac{e^2}{r} \to \frac{e^2}{r}\ \exp\{-\mu\, r\}, \tag{31}$$

where μ is the screening mass specifying the Debye or screening radius $r_D = 1/\mu$. In a plasma of color-charged constituents, one expects a similar behavior, and this is indeed observed in lattice studies [56]: in the QGP just above T_c, μ increases strongly, more than linearly, and hence r_D decreases correspondingly. Asymptotically, perturbation theory suggests $\mu \simeq g(T)T$, with $g(T)$ for the strong coupling running in temperature. The range of strong interactions thus shows a striking in-medium decrease for increasing temperature.

Quarkonia are a special kind of hadrons, bound states of a heavy (c or b) quark and its antiquark. For the ground states J/ψ and Υ the binding energies are around 0.6 and 1.2 GeV, respectively, and thus much larger than the typical hadronic scale $\Lambda \sim 0.2$ GeV; as a consequence, they are also much smaller, with radii r_Q of about 0.1 and 0.2 fm. The fate of such states in a quark-gluon plasma therefore depends on the relative size of the color screening radius: if $r_D \gg r_Q$, the medium does not really affect the heavy quark binding.

Once $r_D \ll r_Q$, however, the two heavy quarks cannot "see" each other any more and hence the bound state will melt [57]. It is therefore expected that quarkonia will survive in a quark-gluon plasma through some range of temperatures above T_c, and then melt once T becomes large enough. Such behavior is in fact confirmed by finite temperature lattice QCD studies of in-medium quarkonium behavior [58].

The higher excited quarkonium states are less tightly bound and hence larger, although their binding energies are in general still larger, their radii still smaller, than those of the usual light quark hadrons. Take the charmonium spectrum as example: the radius of the J/ψ(1S) is about 0.2 fm, that of the χ_c(1P) about 0.3 fm, and that of the ψ'(2S) 0.4 fm. Since melting sets in when the screening radius reaches the binding radius, We expect that the different charmonium states have different "melting temperatures" in a quark-gluon plasma. Hence the spectral analysis of in-medium quarkonium dissociation should provide a QGP thermometer [59, 60].

As probe, we then shoot beams of specific charmonia (J/ψ, χ_c, ψ') into our medium sample and check which comes out on the other side. If all three survive, we have an upper limit on the temperature, and by checking at just what temperature the ψ', the χ_c and the J/ψ are dissociated, we have a way of specifying the temperature of the medium [60], as illustrated in Fi. 17.

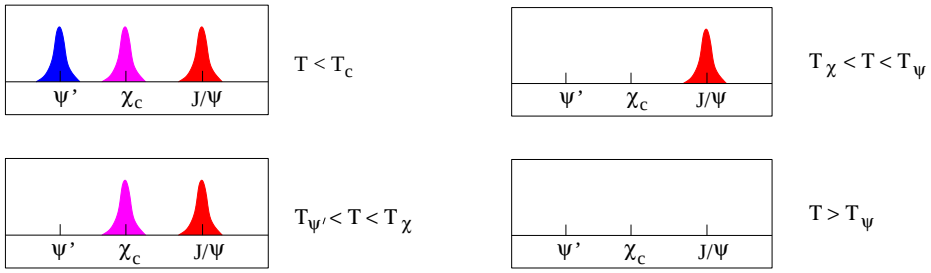

Figure 17: Charmonia as thermometer

The dissociation of quarkonium states in a deconfined medium, as compared to their survival in hadronic matter, can also be considered on a more dynamical level, using the J/ψ as example. The J/ψ is a hadron with characteristic short-distance features; in particular, rather hard gluons are necessary to resolve or dissociate it, making such a dissociation accessible to perturbative calculations. J/ψ collisions with ordinary hadrons made up of the usual u, d and s quarks thus probe the local partonic structure of these 'light' hadrons, not their global hadronic aspects, such as mass or size. It is for this reason that J/ψ's can be used as a confinement/deconfinement probe.

This can be illustrated by a simple example. Consider an ideal pion gas as a confined medium. The momentum spectrum of pions has the Boltzmann form $f(p) \sim \exp -(|p|/T)$, giving the pions an average momentum $\langle |p| \rangle = 3\ T$. With the pionic gluon distribution function $xg(x) \sim (1-x)^3$, where $x = k/p$ denotes the fraction of the pion momentum carried by a gluon, the average momenta of gluons confined to pions becomes

$$\langle |k| \rangle_{\rm conf} \simeq 0.6\ T. \tag{32}$$

On the other hand, an ideal QGP as prototype of a deconfined medium gives the gluons themselves the Boltzmann distribution $f(k) \sim \exp -(|k|/T)$ and hence average momenta

$$\langle |k| \rangle_{\rm deconf} = 3\ T. \tag{33}$$

Deconfinement thus results in a hardening of the gluon momentum distribution. More generally speaking, the onset of deconfinement will lead to parton distribution functions which are different from those in vacuum, as determined by deep inelastic scattering experiments. Since hard gluons are needed to resolve and dissociate J/ψ's, one can use J/ψ's to probe the in-medium gluon hardness and hence the confinement status of the medium.

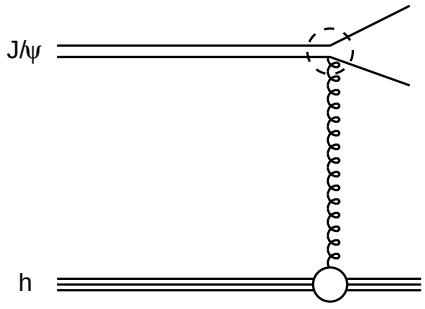

Figure 18: J/ψ dissociation by hadron interaction.

These qualitative considerations can be put on a solid theoretical basis provided by short-distance QCD [61–63]. In Fig. 18 we show the relevant diagram for the calculation of the inelastic J/ψ-hadron cross section, as obtained in the operator product expansion (essentially a multipole expansion for the charmonium quark-antiquark system). The upper part of the figure shows J/ψ dissociation by gluon interaction; the cross section for this process,

$$\sigma_{g-J/\psi} \sim (k - \Delta E_\psi)^{3/2} k^{-5}, \tag{34}$$

constitutes the QCD analogue of the photo-effect. Convoluting the J/ψ gluon-dissociation with the gluon distribution in the incident hadron, $xg(x) \simeq 0.5(1-x)^{1+n}$, we obtain

$$\sigma_{h-J/\psi} \simeq \sigma_{\rm geom}(1 - \lambda_0/\lambda)^{n+3.5} \tag{35}$$

for the inelastic J/ψ-hadron cross section, with $\lambda \simeq (s - M_\psi^2)/M_\psi$ and $\lambda_0 \simeq (M_h + \Delta E_\psi)$; s denotes the squared J/ψ-hadron collision energy. In Eq. (35), $\sigma_{\rm geom} \simeq$ const. $r_\psi^2 \simeq 2 - 3$ mb is the geometric cross section attained at high collision energies with the mentioned gluon distribution. In the threshold region and for relatively low collision energies, $\sigma_{h-J/\psi}$ is very strongly damped because of the suppression $(1-x)^{1+n}$ of hard gluons in hadrons, which leads to the factor $(1 - \lambda_0/\lambda)^{n+3.5}$ in Eq. (35). In Fig. 19, we compare the cross sections for J/ψ dissociation by gluons ("gluo-effect") and by pions ($n = 2$), as given by Eq's (34) and (35). Gluon dissociation shows the typical photo-effect form, vanishing until the gluon momentum k passes the binding energy ΔE_ψ; it peaks just a little later and then vanishes again when sufficiently hard gluons just pass through the much larger charmonium bound states. In contrast, the J/ψ-hadron cross section remains negligibly small until rather high hadron momenta (3 - 4 GeV). In a thermal medium, such momenta correspond to temperatures of more than one GeV. Hence confined media in the temperature range of a few hundred MeV are essentially transparent to J/ψ's, while deconfined media of the same temperatures very effectively dissociate them and thus are J/ψ-opaque.

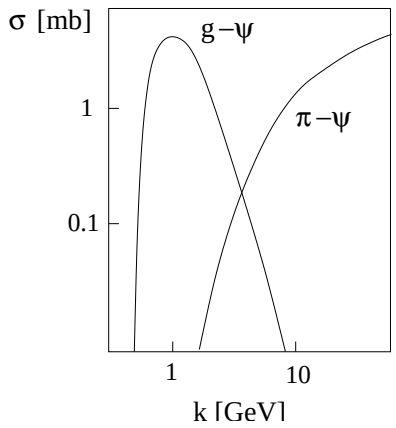

Figure 19: J/ψ dissociation by gluons and by pions; k denotes the momentum of the projectile incident on a stationary J/ψ.

6.4 Jet Quenching

Another possible probe is to shoot an energetic parton, quark or gluon, into our medium to be tested. How much energy it loses when it comes out on the other side will tell us something about the density of the medium [64]. In particular, the density in a quark-gluon plasma is by an order of magnitude or more higher than that of a confined hadronic medium, and so the energy loss of a fast passing color charge is expected to be correspondingly higher as well. Let us consider this in more detail.

An electric charge, passing through matter containing other bound or unbound charges, loses energy by scattering. For charges of low incident energy E, the energy loss is largely due to ionization of the target matter. For sufficiently high energies, the incident charge scatters directly on the charges in matter and as a result radiates photons of average energy $\omega \sim E$. Per unit length of matter, the 'radiative' energy loss due to successive scatterings,

$$-\frac{dE}{dz} \sim E \tag{36}$$

is thus proportional to the incident energy.

This probabilistic picture of independent successive scatterings breaks down at very high incident energies [65]. The squared amplitude for n scatterings now no longer factorizes into n interactions; instead, there is destructive interference, which for a regular medium (crystal) leads to a complete cancellation of all photon emission except for the first and last of the n photons. This Landau-Pomeranchuk-Migdal (LPM) effect greatly reduces the radiative energy loss.

The physics of the LPM effect is clearly relevant in calculating the energy loss for fast color charges in QCD media. These media are not regular crystals, so that the cancellation becomes only partial. Let us consider the effect here in a heuristic fashion; for details of the actual calculations, see [66, 67]. The time t_c needed for the emission of a gluon after the scattering of a quark (see Fig. 20) is given by

$$t_c = \frac{1}{\sqrt{P^2}} \frac{E}{\sqrt{P^2}} = \frac{E}{2P'k}, \tag{37}$$

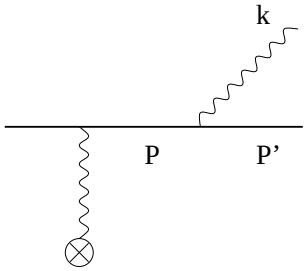

Figure 20: Gluon emission after scattering.

in the rest system of the scattering center, where P^2 measures how far the intermediate quark state is off-shell; on-shell quarks and gluons are assumed to be massless, and $E/\sqrt{P^2}$ is the γ-factor between the lab frame and the proper frame of the intermediate quark. For gluons with $k_L >> k_T$, we thus get

$$t_c \simeq \frac{\omega}{k_T^2}. \tag{38}$$

If the passing color charge can interact with several scattering centers during the formation time of a gluon, the corresponding amplitudes interfere destructively, so that in effect after the passage of n centers over the coherence length z_c, only one gluon is emitted, in contrast to the emission of n gluons in the incoherent regime. Nevertheless, in both cases each scattering leads to a k_T-kick of the charge, so that after a random walk past n centers, $k_T^2 \sim n$. Hence

$$k_T^2 \simeq \mu^2 \frac{z_c}{\lambda}, \tag{39}$$

where λ is the mean free path of the charge in the medium, so that $z_c/\lambda > 1$ counts the number of scatterings. At each scattering, the transverse kick received is measured by the mass of the gluon exchanged between the charge and the scattering center, i.e., by the screening mass μ of the medium. From Eq. 38 we have

$$z_c \simeq \frac{\omega}{k_T^2}, \tag{40}$$

so that the formation length in a medium characterized by μ and λ becomes

$$z_c \simeq \sqrt{\frac{\lambda}{\mu^2}\omega}. \tag{41}$$

For the validity of Eq. (41), the mean free path has to be larger than the interaction range of the centers, i.e., $\lambda > \mu^{-1}$.

The energy loss of the passing color charge is now determined by the relative scales of the process. If $\lambda > z_c$, we have incoherence, while for $\lambda < z_c$ there is coherent scattering with destructive interference. In both cases, we have assumed that the thickness L of the medium is larger than all other scales. When the coherence length reaches the size of the system, $z_c = L$, effectively only one gluon can be emitted. This defines a critical thickness $L_c(E) = (E\lambda/\mu^2)^{1/2}$ at fixed incident energy E, or equivalently a critical $E_c = \mu^2 L^2/\lambda$ for fixed thickness L; for $L > L_c$, there is bulk LPM-behavior, below L_c there are finite-size corrections.

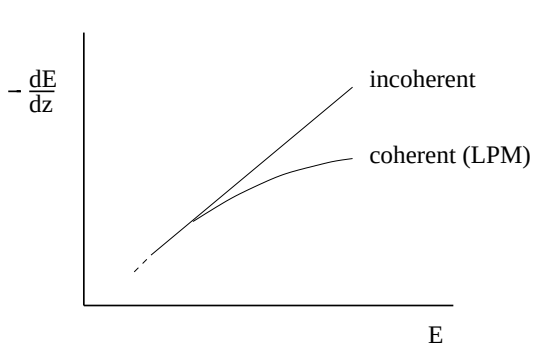

Figure 21: Energy loss in incoherent and coherent interactions.

We are thus left with three regimes for radiative energy loss. In case of incoherence, $z_c < \mu^{-1}$, there is the classical radiative loss

$$-\frac{dE}{dz} \simeq \frac{3\alpha_s}{\pi}\frac{E}{\lambda}, \tag{42}$$

where α_s is the strong coupling. In the coherent region, $\lambda > z_c$, the energy loss is given by the LPM bulk expression when $L > L_c$ [66],

$$-\frac{dE}{dz} \simeq \frac{3\alpha_s}{\pi}\sqrt{\frac{\mu^2 E}{\lambda}}. \tag{43}$$

The resulting reduction in the radiative energy loss dE/dz is illustrated in Fig. 21. Note that in earlier estimates the energy loss due to interactions of the gluon cloud accompanying the passing color charge had been neglected [68]; this led to a considerably smaller energy loss, proportional to $\ln E$ instead of $\sqrt{E}$. Finally, in a medium of thickness $L < L_c$, there is less scattering and hence still less energy loss. Eq. (43) can be rewritten as

$$-\frac{dE}{dz} \simeq \frac{3\alpha_s}{\pi}\frac{\mu^2}{\lambda}L_c(E), \tag{44}$$

and for $L < L_c$, this leads to

$$-\frac{dE}{dz} \simeq \frac{3\alpha_s}{\pi}\frac{\mu^2}{\lambda}L \tag{45}$$

as the energy loss in finite size media with $L \leq L_c$. The resulting variation of the radiative energy loss with the thickness of the medium is shown in Fig. 22, with saturated (i.e., bulk) LPM behavior setting in for $L \geq L_c$.

Eq. (45) has been used to compare the energy loss in a deconfined medium of temperature $T = 0.25$ GeV to that in cold nuclear matter of standard density [69]. For the traversal of a medium of 10 fm thickness, estimates give for the total energy loss

$$\Delta E = \int_{0\ \mathrm{fm}}^{10\ \mathrm{fm}} dz \frac{dE}{dz} \tag{46}$$

in a quark-gluon plasma

$$-\Delta E_{qgp} \simeq 30\ \ \mathrm{GeV}, \tag{47}$$

corresponding to an average loss of 3 GeV/fm. In contrast, cold nuclear matter leads to

$$-\Delta E_{cnm} \simeq 2\ \ \mathrm{GeV} \tag{48}$$

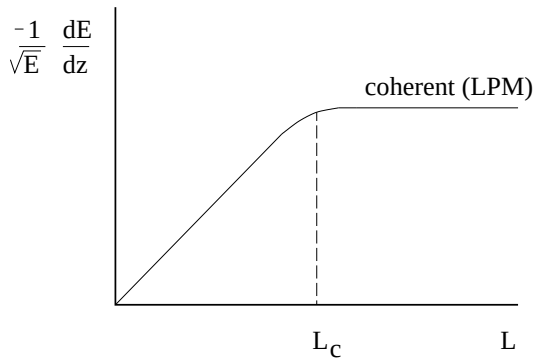

Figure 22: Energy loss in coherent interactions as function of the thickness L of the medium

and hence an average loss of 0.2 GeV/fm. A deconfined medium thus leads to a very much higher rate of jet quenching than confined hadronic matter, as had in fact been suggested quite some time ago [64].

6.5 Initial State Considerations

In using quarkonia and jets as tools, we have so far again considered a simplified situtation, in which we test a given medium with distinct external probes. In heavy ion collisions, we have to create the probe in the same collision in which we create the medium. Quarkonia and jets (as well as open charm/beauty and very energetic dileptons and photons) constitute so-called "hard probes", whose production occurs at the very early stages of the collision, before the medium is formed; they are therefore present when it appears. Moreover, their production involves large energy/momentum scales and can be calculated by perturbative QCD techniques; the results can be tested in pp/pA collisions, so that behavior and strength of such outside "beams" or "color charges" are in principle under control.

On the other hand, such calculations based on hard partonic interactions assume

- that the parton distributions function in nuclei are known, and
- that the parton model itself is applicable for nuclear collisions.

Both assumptions cannot be universally valid. The parton distribution functions are modified in nuclei because of the presence of other parton sources (shadowing, anti-shadowing), and these effects are to a considerable extent of non-perturbative nature. Moreover, the number of partons, and hence their density in the transverse plane, increase with collision energy. Partons with an intrinsic transverse momentum have an intrinsic size in the transverse plane, and so increasing their density will eventually lead to parton saturation. This is another instance of the percolation process discussed above. At this point of "parton saturation", any model of independent partonic interactions breaks down, and we have a new medium. The study of such saturation effects has in recent years attracted much attention ("color glass condensate") [70, 71] and will be dealt with in other chapters of this handbook.

As already mentioned, another crucial aspect for the formation of a quark-gluon plasma in high energy nuclear collisions is the question of how a locally equilibrated medium can be formed from a non-equilibrium initial state. This question arises for a partonic initial state (parton thermalization) as well for the possible transition of a primary saturated medium

to a quark-gluon plasma, with a possible futher intermediate state ("glasma") [71, 72]. Here again we refer to subsequent chapters.

7 Summary

We have shown that strong interaction thermodynamics results in a well-defined transition from hadronic matter to a plasma of deconfined quarks and gluons. For vanishing baryon number density, the transition provides both deconfinement and chiral symmetry restoration at $T_c \simeq 160 - 190$ MeV. At this point, the energy density increases by an order of magnitude through the latent heat of deconfinement.

The behavior of strongly interacting matter for increasing baryon density is presently at the focus of much attention; both the change of the transition nature with μ and the origin for the expected changes have to be clarified further.

The properties of the new medium above T_c, the quark-gluon plasma, can be studied through hard probes (quarkonium dissociation, jet quenching) and electromagnetic radiation (photons and dileptons). Information about transition aspects is provided by light hadron radiation; in particular, experimental species abundances show a universal hadronization temperature in accord with that found in non-perturbative QCD studies.

References

[1] W. Heisenberg, Z. Phys. 101 (1936) 533; Z. Phys. 113 (1939) 61.

[2] E. Fermi, Progr. Theor. Phys. (Japan) 5 (1950) 570.

[3] I. Ya. Pomeranchuk, Doklady Akad. Nauk. SSSR 78 (1951) 889.

[4] L. D. Landau, Izv. Akad. Nauk SSSr 17 (1953) 51.

[5] R. Hagedorn, Nuovo Cim. Suppl. 3 (1965) 147;
Nuovo Cim. 56A (1968) 1027.

[6] G. Veneziano, Nuovo Cim. 57A (1968) 190;
K. Bardakci and S. Mandelstam, Phys. Rev. 184 (1969) 1640;
S. Fubini and G. Veneziano, Nuovo Cim. 64A (1969) 811.

[7] N. Cabbibbo and G. Parisi, Phys. Lett. 59 B (1975) 67.

[8] H. Satz, Fortsch. Physik 33 (1985) 259.

[9] See e.g., M. G. Alford et al., Rev. Mod. Phys. 80 (2008) 1455.

[10] L. McLerran and R. Pisarski, Nucl. Phys. A 796 (2007) 83;
L. McLerran, K. Redlich and C. Sasaki, arXiv:0812.3585.

[11] P. Castorina, K. Redlich and H. Satz, Europ. Phys. J. C 59 (2009) 67.

[12] A. Chodos, R.L. Jaffe, K. Johnson, C.B. Thorn and V.F. Weisskopf, Phys. Rev. D9 (1974) 3471.

[13] M. Asakawa and T. Hatsuda, Nucl. Phys. A 610 (1996) 470c.

[14] K. Wilson, Phys. Rev. D10 (1974) 2445.

[15] M. Creutz, Phys. Rev. D 21 (1980) 2308.

[16] For textbooks, surveys and further literature, see
I. Montvay and G. Münster, *Quantum Fields on a Lattice*, Cambridge University Press 1994;
H. J. Rothe, *Lattice Gauge Theory*, World Scientific Lecture Notes in Physics 59 (1997);
F. Karsch, Lect. Notes Phys. (Springer) 583 (2002) 209;
F. Karsch and E. Laermann, in *Quark-Gluon Plasma 3*, R. C. Hwa and X.-N. Wand (Eds.), World Scientific, Singapore 2004;
F. Karsch, arXiv[hep-lat] 0711.0661 and 0711.0656.

[17] L. D. McLerran and B. Svetitsky, Phys. Lett. 98 B (1981) 195 and Phys. Rev. D 24 (1981) 450.

[18] J. Kuti, J. Polónyi and K. Szlachányi, Phys. Lett. 98B (1981) 199.

[19] B. Svetitsky and L. G. Yaffe, Nucl. Phys. B 210 [FS6] (1982) 423.

[20] F. Karsch and E. Laermann, Phys. Rev. D 50 (1994) 6954.

[21] M. Cheng et al., Phys. Rev. D 75 (2007) 034506.

[22] M. Cheng et al., Phys. Rev. D 77 (2008) 014511.

[23] Y. Aoki et al., Phys. Lett. B 643 (2006) 46.

[24] J. Engels et al., Phys. Lett. 101B (1981) 89 and Nucl. Phys. B205 (1982) 545

[25] F. Karsch, E. Laermann and A. Peikert, Phys. Lett. B 478 (2000) 447.

[26] C. Aubin et al. (MILC Collaboration), Phys. Rev. D70 (2004) 094505;
A. Gray et al., Phys. Rev. D72 (2005) 0894507,
M. Cheng et al., Phys. Rev. D74 (2006) 054507.

[27] M. A. Shifman, in *QCD - 20 Years Later*, P. M. Zerwas and H. A. Kastrup (Edts.), World Scientific, Singapore 1993, Vol. 2, 775.

[28] M. A. Shifman, A. I. Vainshtein and V. I. Zakharov, Nucl. Phys. B 147 (1979) 385.

[29] H. Leutwyler, in *QCD - 20 Years Later*, P. M. Zerwas and H. A. Kastrup (Edts.), World Scientific, Singapore 1993, Vol. 2, 693.

[30] G. Boyd et al., Nucl. Phys. B 469 (1996) 419.

[31] M. D'Elia, A. Di Giacomo and E. Meggiolaro, Phys. Rev. D 67 (2003) 114504.

[32] V. Goloviznin and H. Satz, Z. Phys. C 57 (1993) 671.

[33] F. Karsch, A. Patkos and P. Petreczky, Phys. Lett. B 401 (1997) 69.

[34] R. D. Pisarski and F. Wilczek, Phys. Rev. D29 (1984) 338.

[35] F. Karsch, E. Laermann and C. Schmidt, Phys. Lett. B520 (2001) 41.

[36] S. Gavin, A. Goksch and R. D. Pisarski, Phys. Rev. D49 (1994) 3079.

[37] K. Redlich and H. Satz, Phys. Rev. D 33 (1986) 3747.

[38] M. Halasz et al., Phys. Rev. D 58 (1998) 096007;
M. Stephanov, K. Rajagopal and E. Shuryak, Phys. Rev. Lett. 81 (19989) 4816.

[39] Z. Fodor and S. Katz, JHEP 0203 (2002) 014.

[40] C. R. Allton et al., Phys. Rev. D 68 (2003) 014507;
C. Miau and C. Schmidt, PoS (LATTICE 2007) 175.

[41] R. V. Gavai and S. Gupta, Phys. Rev. D68 (2003) 034506; Phys. Rev. D71 (2005) 114014; Phys. Rev. D78 (2008) 114503.

[42] P. de Forcrand and O. Philipsen, Nucl. Phys. B 642 (2002) 290.

[43] M.-P. Lombardo, Phys. Rev. D 67 (2003) 014505.

[44] G. Baym, Physics 96A (1979) 131;
T. Çelik, F. Karsch and H. Satz, Phys. Lett. 97B (1980) 128;
H. Satz, Nucl. Phys. A642 (1998) 130c.

[45] D. Stauffer and A. Aharony, *Introduction to Percolation Theory*, Taylor and Francis, London 1994.

[46] S. Digal, S. Fortunato and H. Satz, Europ. Phys. J. 32 (2004) 547.

[47] C. M. Fortuin, P. W. Kasteleyn J. Phys. Soc. Japan 26 (Suppl.), 11 (1969);
Physica 57, 536 (1972).

[48] See e.g., F. Karsch and H. Satz, Phys. Rev. D 21 (1980) 1168.

[49] K. W. Kratky, J. Stat. Phys. 52 (1988) 1413.

[50] E. Beth and G. E. Uhlenbeck, Physica 4 (1937) 915;
R. Dashen, S. Ma and H. J. Bernstein, Phys. Rev. 187 (1969) 345.

[51] J. Cleymans and H. Satz, Z. Phys. C57 (1993) 135;
K. Redlich et al., Nucl. Phys. A 566 (1994) 391;
P. Braun-Munzinger et al., Phys. Lett. B344 (1995) 43;
F. Becattini, Z. Phys. C69 (1996) 485;
F. Becattini and U. Heinz, Z. Phys. C76 (1997) 268.
For a recent survey, see
P. Braun-Munzinger, K. Redlich and J. Stachel, in *Quark-Gluon Plasma 3*, R. C. Hwa and X.-N. Wang (Edts.), World Scientific Publishing, Singapore 2004.

[52] D. Kharzeev and K. Tuchin, Nucl. Phys. A **753**, 316 (2005);
P. Castorina, D. Kharzeev and H. Satz, Europ. Phys. J. 52 (2007) 187.

[53] S. W. Hawking, Comm. Math. Phys. 43 (1975) 199;
W. G. Unruh, Phys. Rev. D14 (1976) 870;
for a recent survey, see e.g.,
L. C. B. Crispino, A. Higuchi and G. E. A. Matsas, Rev. Mod. Phys. 80 (2008) 787.

[54] L. D. Landau, Izv. Akad. Nauk, Ser. Fiz. 17 (1953) 51;
J.-P. Blaizot and J.-Y. Ollitrault, in *Quark-Gluon Plasma 2*, R. C. Hwa (Ed.), World Scientific, Singapore 1990;
U. Heinz, P. F. Kolb and J. Sollfrank, Phys. Rev. C62 (2000) 054909.

[55] E.V. Shuryak, Phys. Rep. 61 (1980) 71;
K. Kajantie and H.I. Miettinen, Z. Phys. C 9 (1981);
J. Kapusta, Phys. Lett. 136 B (1984) 201,
L. McLerran and T. Toimela, Phys. Rev. D 31 (1985) 545.

[56] S. Digal et al., Europ. Phys. J. 43 (2005) 71;
O. Kaczmarek and F. Zantow, Phys. Rev. D 71 (2005) 114510.

[57] T. Matsui and H. Satz, Phys. Lett. B178 (1986) 416.

[58] S. Datta et al., PR D69 (2004) 094507;
G. Aarts et al., Phys. Rev. D67 (2007) 0945413 and literature given there.

[59] F. Karsch, M. T. Mehr and H. Satz, Z. Phys. C 37 (1988) 617.

[60] F. Karsch and H. Satz, Z. Phys. C 51 (1991) 209.

[61] M. E. Peskin, Nucl. Phys. B156 (1979) 365;
G. Bhanot and M. E. Peskin, Nucl. Phys. B156 (1979) 391.

[62] A. Kaidalov, in *QCD and High Energy Hadronic Interactions*, J. Tran Thanh Van (Ed.), Editions Frontieres, Gif-sur-Yvette, 1993.

[63] D. Kharzeev and H. Satz, Phys. Lett. B 334 (1994) 155.

[64] J.D. Bjorken, Fermilab-Pub-82/59-THY (1982) and Erratum;
M. Gyulassy and X.-N. Wang, Nucl. Phys. B420 (1994) 583;
R. Baier et al., Phys. Lett. B 345 (1995);
B. G. Zakharov, JETP Letters 63 (1996) 952.

[65] L. P. Landau and I. Ya. Pomeranchuk, Doklad. Akad. Nauk SSSR 92 (1953) 535, 735;
A. B. Migdal, Phys. Rev. 103 (1956) 1811;
E. L. Feinberg and I. Ya. Pomeranchuk, Suppl. Nuovo Cim. III, Ser. X, No. 4 (1956) 652.

[66] R. Baier et al., Phys. Lett. B 345 (1995) 277; Nucl. Phys. B 483 (1997) 291; Nucl. Phys. B484 (1997) 265; Nucl. Phys. B 531 (1998) 403.

[67] B. G. Zakharov, JETP Letters 63 (1996) 952; JETP Lett. 65 (1997) 615.

[68] M. Gyulassy and X.-N. Wang, Nucl. Phys. B 420 (1994) 583;
M. Gyulassy, M. Plümer and X.-N. Wang, Phys. Rev. D 51 (1995) 3436.

[69] D. Schiff, Acta Phys. Polon. B 30 (1999) 3621.

[70] L. McLerran and R. Venugopalan, Phys. Rev. D 49 (1994) 2233.

[71] For an introduction, see D. Banerjee, J. K. Nayak and R. Venugopalan, arXiv:0810.3553 (*Springer Lecture Notes in Physics*, in press).

[72] T. Lappi and L. McLerran, Nucl. Phys. A 772 (2006) 200.